*International Journal of Minerals, Metallurgy and Materials*
*Volume 24, Number 3, March 2017, Page 342*
**DOI: 10.1007/s12613-017-1413-6**

# Electrochemical performance of a nickel-rich $LiNi_{0.6}Co_{0.2}Mn_{0.2}O_2$ cathode material for lithium-ion batteries under different cut-off voltages

*Kai-lin Cheng*[1)], *Dao-bin Mu*[1)], *Bo-rong Wu*[1,2)], *Lei Wang*[1)], *Ying Jiang*[1)], *and Rui Wang*[1)]

1) Beijing Key Laboratory of Environmental Science and Engineering, School of Materials Science and Engineering, Beijing Institute of Technology, Beijing 100081, China

2) Collaborative Innovation Center of Electric Vehicles in Beijing, Beijing 100081, China

(Received: 12 October 2016; revised: 31 October 2016; accepted: 2 November 2016)

**Abstract:** A spherical-like $Ni_{0.6}Co_{0.2}Mn_{0.2}(OH)_2$ precursor was tuned homogeneously to synthesize $LiNi_{0.6}Co_{0.2}Mn_{0.2}O_2$ as a cathode material for lithium-ion batteries. The effects of calcination temperature on the crystal structure, morphology, and the electrochemical performance of the as-prepared $LiNi_{0.6}Co_{0.2}Mn_{0.2}O_2$ were investigated in detail. The as-prepared material was characterized by X-ray diffraction, scanning electron microscopy, laser particle size analysis, charge–discharge tests, and cyclic voltammetry measurements. The results show that the spherical-like $LiNi_{0.6}Co_{0.2}Mn_{0.2}O_2$ material obtained by calcination at 900°C displayed the most significant layered structure among samples calcined at various temperatures, with a particle size of approximately 10 μm. It delivered an initial discharge capacity of 189.2 $mAh{\cdot}g^{-1}$ at 0.2C with a capacity retention of 94.0% after 100 cycles between 2.7 and 4.3 V. The as-prepared cathode material also exhibited good rate performance, with a discharge capacity of 119.6 $mAh{\cdot}g^{-1}$ at 5C. Furthermore, within the cut-off voltage ranges from 2.7 to 4.3, 4.4, and 4.5 V, the initial discharge capacities of the calcined samples were 170.7, 180.9, and 192.8 $mAh{\cdot}g^{-1}$, respectively, at a rate of 1C. The corresponding retentions were 86.8%, 80.3%, and 74.4% after 200 cycles, respectively.

**Keywords:** lithium-ion batteries; cathodic materials; calcination; electrochemical properties

## 1. Introduction

Lithium-ion batteries (LIBs) have become one of the most feasible alternatives for power sources in portable electronic devices and electrical vehicles because of their high discharge capacity, high operating voltage, good cycling performance, and long cycle life [1–3]. However, their further development is limited by issues such as the limited charge capacity of the electrode materials and complex manufacturing processes; one of the bottlenecks is the cathode material [4–5].

Recently, nickel-rich layered $LiNi_xCo_yMn_{1-x-y}O_2$ ($x \geq 0.6$) cathode materials have attracted much attention because of their high specific capacity and low cost [6–8]. With increasing Ni content, the specific capacity of $LiNi_xCo_yMn_{1-x-y}O_2$ increases but the thermal and cycling stabilities decrease [9–10]. Among various nickel-rich layered Mn based cathode materials, $LiNi_{0.6}Co_{0.2}Mn_{0.2}O_2$ (NCM622) has been investigated as a promising candidate. Various approaches have been used to synthesize the cathode material, such as co-precipitation [11–15], solid-state reaction [16–18], spray-drying [19–20], and sol–gel methods [21–23]. The co-precipitation approach, which is widely used, offers advantages with respect to morphology control and feasibility. The NCM622 prepared by Cao *et al.* [24] via this method delivered an initial discharge capacity of 170 $mAh{\cdot}g^{-1}$ between 2.7 and 4.3 V and a capacity greater than 151 $mAh{\cdot}g^{-1}$ after 70 cycles. However, the capacity decayed rapidly upon further cycling. By optimizing the co-precipitation conditions such as pH, the concentration of $NH_4OH$, and the stirring speed, Liang *et al.* [25] prepared NCM622 with a well-ordered layered structure; this material exhibited an initial discharge capacity of 172.1 $mAh{\cdot}g^{-1}$ with 90.1% capacity retention after 100 cycles between 2.7 and 4.3 V. In general, the nickel-rich layered NCM622 cathode material demonstrates high capacity; however, its

Corresponding author: Dao-bin Mu E-mail: mudb@bit.edu.cn

cycling performance, especially under higher voltages [26–28], is unsatisfactory.

With increasing charge cut-off voltage, the capacity of the NCM622 cathode material increases; however, its structure becomes unstable because of the dissolution of transition-metal cations from the material into the electrolyte and the formation of a solid electrolyte interphase (SEI) [27,29]. Cobalt dissolution at higher operating voltages (> 4.3 V) has been reported to be an important factor with respect to cycling performance [30]. In addition, the tap-density and particle morphology of the precursors strongly influence the lithium insertion/extraction properties of the NCM622 material. These factors would unavoidably affect the electrochemical performance of the nickel-rich NCM622 cathode material.

In this work, an $Ni_{0.6}Co_{0.2}Mn_{0.2}(OH)_2$ precursor was tuned uniformly to synthesize nickel-rich NCM622 cathode material. The effects of calcination temperature on the structure, morphology, and electrochemical performance of the material were investigated in detail. Importantly, the electrochemical performance of the as-prepared NCM622 cathode material was also examined within the voltage ranges from 2.7 to 4.3, 4.4, and 4.5 V.

## 2. Experimental

### 2.1. Material synthesis

$NiSO_4 \cdot 6H_2O$, $CoSO_4 \cdot 7H_2O$, $MnSO_4 \cdot H_2O$, NaOH, and $NH_4 \cdot OH$ were used as the starting materials to prepare $Ni_{0.6}Co_{0.2}Mn_{0.2}(OH)_2$ precursor. A 2 $mol \cdot L^{-1}$ aqueous solution of transition-metal sulfates ($Ni^{2+}$: $Co^{2+}$: $Mn^{2+}$ = 6:2:2, molar ratio) was pumped into a continuously stirred tank reactor (1 L) at a stable flow rate under an argon atmosphere; 4 $mol \cdot L^{-1}$ NaOH (aq) and a moderate amount of $NH_4 \cdot OH$ (aq) as chelating agents were also slowly pumped into the reactor. The pH of the mixed solution was adjusted to 11, and the stirring speed was maintained at 1000 r/min. After reacting for 12 h, the obtained precursor was washed several times with distilled water to remove the residual salt ions. The precipitates were then dried at 80°C for 12 h. The concentration and pH of the solution, the amount of $NH_4OH$, and the stirring speed and temperature in the reactor were carefully tuned.

The as-prepared precursor and excess amount of $Li_2CO_3$ were mixed thoroughly. The mixture was first heated at 550°C for 4 h and then calcined at 700, 750, 800, 850, 900, and 950°C for 12 h in air to synthesize NCM622 material.

### 2.2. Characterization

X-ray diffraction (XRD) patterns of the samples were recorded using an Ultima IV diffractometer (UltimaIV-185, Rigaku) with a filtered Cu $K_\alpha$ radiation source (scan rate: 0.5°·$min^{-1}$, scan range: 10°–80°). The morphologies of the prepared materials were examined by scanning electron microscopy (JEOL JSM-5600LV). Particle size analysis was carried out using a laser particle size analyzer (LS-POP(9)).

### 2.3. Electrochemical tests

Electrochemical measurements were performed at room temperature using CR2025 coin-type cells. The working electrode was prepared by mixing the as-prepared NCM622, Super P carbon black, and polyvinylidene fluoride in a mass ratio of 8:1:1. The mixture was then dissolved in *N*-methyl-2-pyrrolidone (NMP) to form a slurry. The mixed slurry was pasted uniformly using a doctor blade onto an aluminum foil and dried at 80°C for 10 h. Electrodes were punched from the coated foil in the form of 12-mm-diameter disks. The cells were assembled in an argon-filled glove box. A solution of 1 $mol \cdot L^{-1}$ $LiPF_6$/EC + DEC (EC: DEC = 1:1 in mass ratio) was used as the electrolyte, Celgard 2300 film was used as the separator, and a Li sheet was used as the counter electrode.

The charge–discharge tests were carried out under different cut-off voltage ranges from 2.7 to 4.3, 4.4, and 4.5 V at 0.2C and 1C (1C = 180 $mA \cdot g^{-1}$) using a LAND 2001 CT battery tester. Cyclic voltammetry (CV) of the cathodes was performed at a scan rate of 0.1 $mV \cdot s^{-1}$ between 2.7 and 4.3 V.

## 3. Results and discussion

### 3.1. Physical performance of the as-prepared materials

Fig. 1(a) shows the XRD pattern of the as-prepared precursor. It is indexed to a hexagonal structure with a space group of $P\bar{3}m1$, similar to the indexing of the pattern of $Ni(OH)_2$ [7]. The lattice parameters of the precursor are $a$ = 0.30079 nm and $c$ = 0.47716 nm. This result indicates that $Co^{2+}$ and $Mn^{2+}$ ions partially replace $Ni^{2+}$ ions in the $Ni(OH)_2$ structure [31], which demonstrates that the $Ni_{0.6}Co_{0.2}Mn_{0.2}(OH)_2$ precursor was successfully prepared, as noted by other authors [25,32]. Fig. 1(b) presents the XRD patterns of the as-synthesized materials calcined at temperatures of 700, 750, 800, 850, 900, and 950°C. The diffraction peaks are assigned to the (003), (101), (006), (102), (104), (105), (107), (108), (110), and (113) planes of NCM622 (JPCDS No. 09-0063); no extra diffraction peaks are evident. They are all indexed to the $\alpha$-$NaFeO_2$ structure with $R3m$ (166) symmetry. The splitting of the (006)/(102) and (108)/(110) peaks implies the formation of a layered

structure [33]. With increasing calcination temperature, the peak splitting becomes clearer, which indicates more extensive layering [34]. The lattice parameters of the samples are summarized in Table 1 for comparison of the crystallinity of the materials. The values of *a*, *c*, and *V* were calculated on the basis of Bragg's law. The *c* value represents the metal–metal interslab distance, and the *c*/*a* value represents the degree of trigonal distortion [35]. A good hexagonal layered structure is achieved when the *c*/*a* ratio is greater than 4.899 [36]. The lattice parameters (*a*, *c*, and *V*) increase with increasing calcination temperature from 700 to 900°C, as shown in Table 1, which is in agreement with the crystal growth theory [14]. Notably, the material calcined at 900°C exhibits a larger *c*/*a* value (4.961) than the other materials, indicating that its structure exhibits the most extensive layering.

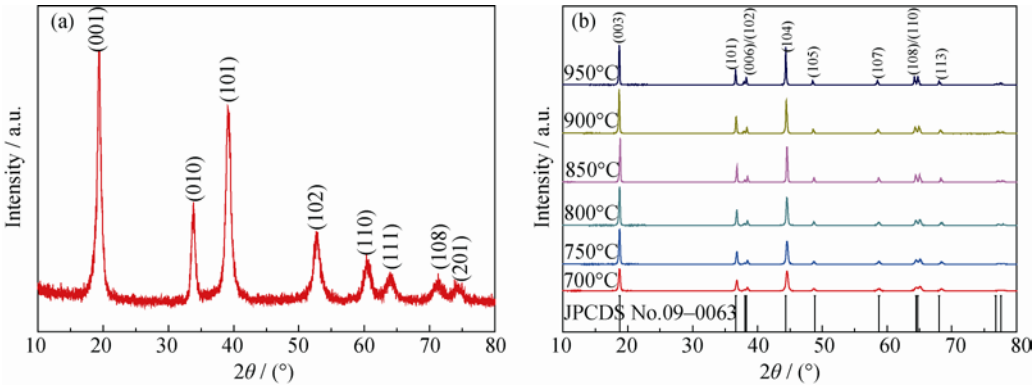


**Fig. 1. XRD patterns of (a) the as-prepared precursor and (b) the as-prepared NCM622 material calcined at different temperatures.**

**Table 1. Lattice parameters of NCM622 samples calcined at different temperatures**

| Temperature / °C | *a* / nm | *c* / nm | *c*:*a* | *V* / nm$^3$ | $I_{003}/I_{104}$ | $(I_{006}+I_{102})/I_{101}$ |
|---|---|---|---|---|---|---|
| 700 | 0.28602 | 1.41745 | 4.956 | 0.10098 | 1.121 | 0.526 |
| 750 | 0.28636 | 1.41944 | 4.957 | 0.10097 | 1.262 | 0.511 |
| 800 | 0.28637 | 1.42031 | 4.959 | 0.10110 | 1.343 | 0.508 |
| 850 | 0.28645 | 1.42024 | 4.958 | 0.10119 | 1.397 | 0.483 |
| 900 | 0.28711 | 1.42435 | 4.961 | 0.10161 | 1.481 | 0.472 |
| 950 | 0.28686 | 1.42060 | 4.952 | 0.10215 | 1.157 | 0.547 |

The intensity ratio of the (003) and (104) peaks ($I_{003}/I_{104}$) is a parameter used to evaluate cation mixing. A ratio less than 1.2 implies a high degree of cation mixing [19]; thus, higher ratios indicate a lower degree of cation mixing [37]. The $I_{003}/I_{104}$ ratio is 1.262, 1.343, 1.397, and 1.481 for the samples calcined at 750, 800, 850, and 900°C, respectively. The $I_{003}/I_{104}$ ratios of these four samples are all greater than 1.2, indicating that the as-synthesized materials exhibit well-ordered, layered $\alpha$-$NaFeO_2$ structures. However, in the case of samples calcined at 700 or 950°C, the $I_{003}/I_{104}$ ratios are less than 1.2, indicating a certain degree of cation mixing; thus, their layer structures are not well-ordered.

The peak intensity ratio of $(I_{006}+I_{102})/I_{101}$ is an indicator of hexagonal ordering [38]. Specifically, a lower $(I_{006}+I_{102})/I_{101}$ ratio indicates better hexagonal ordering. The $(I_{006}+I_{102})/I_{101}$ of the material calcined at 900°C exhibits the lowest value among all of the calcined materials, indicating that this material has the most extensively layered structure. We therefore expected the NCM622 material calcined at 900°C to exhibit good electrochemical performance. Achieving a well-ordered layered structure of the NCM622 material with an appropriate calcination temperature is critical to attaining good electrochemical performance.

Fig. 2 shows the SEM images of the $Ni_{0.6}Co_{0.2}Mn_{0.2}(OH)_2$ precursor and the morphologies of NCM622 samples calcined at different temperatures. The $Ni_{0.6}Co_{0.2}Mn_{0.2}(OH)_2$ precursor clearly exhibits a spherical-like morphology, and its particle size is approximately 10 μm, with a uniform distribution. Importantly, the spherical-like morphology is retained after calcination. Figs. 2(c)–2(i) shows that the primary particle size increases with increasing temperature. For larger particles, the migration distance of lithium ions may increase, resulting in the central parts of the active material particles not being fully utilized. This size effect may adversely influence the insertion/extraction of lithium ions, leading to a decrease of the specific capacity of the cathode material. Compared to the particles prepared at 950°C (Fig. 2(i)), which agglomerate to a certain degree, the NCM622

material calcined at 900°C retains the spherical-like morphology and uniform dispersion of the precursor, as shown in Figs. 2(g) and 2(h). Fig. 3 presents the particle size distribution of the sample calcined at 900°C. The $D_{10}$, $D_{50}$, and $D_{90}$ are 8, 10, and 13 μm, respectively, which demonstrates that the particle size is in normal distribution.

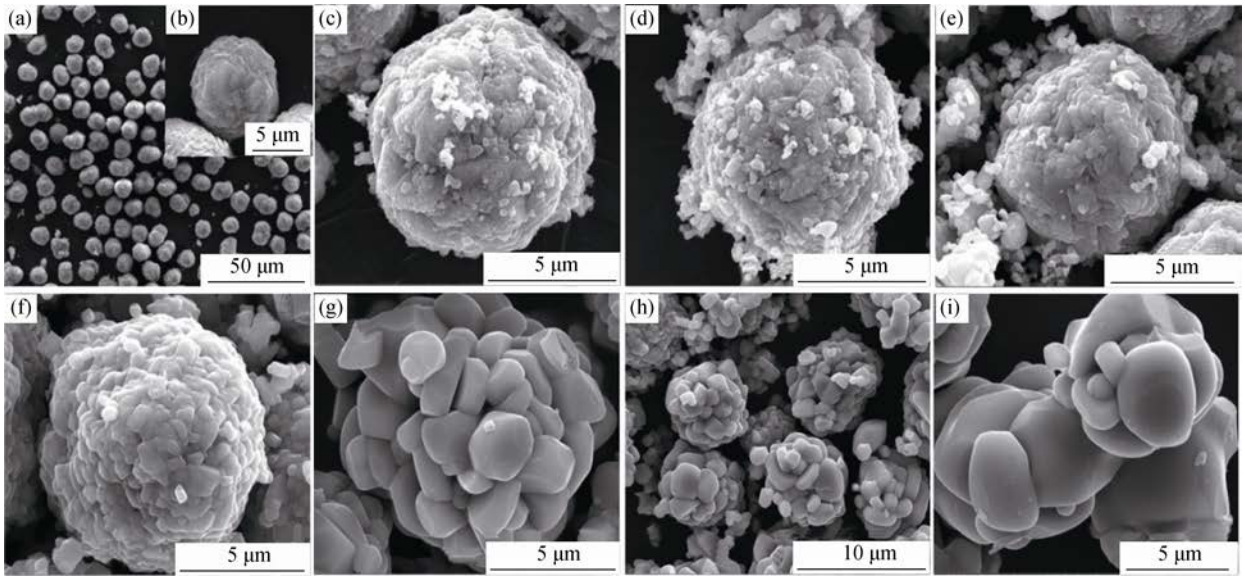


**Fig. 2. SEM images of (a, b) the $Ni_{0.6}Co_{0.2}Mn_{0.2}(OH)_2$ precursor and (c–i) the NCM622 samples calcined at different temperatures: (c) 700°C; (d) 750°C; (e) 800°C; (f) 850°C; (g, h) 900°C; (i) 950°C.**

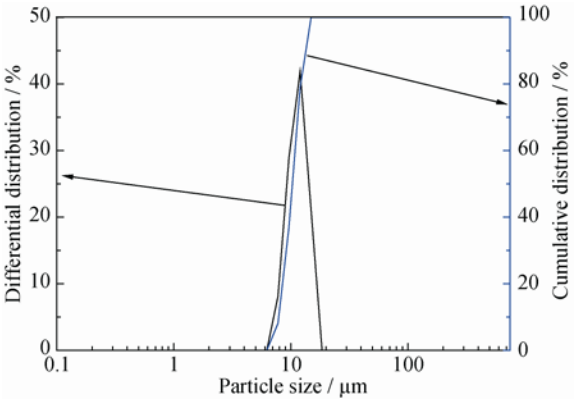


**Fig. 3. Particle size distribution of NCM622 calcined at 900°C.**

### 3.2. Electrochemical performance of the as-prepared materials

3.2.1. Electrochemical performance of NCM622 samples prepared at different temperatures

Fig. 4(a) shows the initial charge and discharge curves of the samples synthesized at various calcination temperatures and cycled at a 0.2C rate between 2.7 and 4.3 V. As displayed, the discharge capacity increases with increasing calcination temperature from 700 to 900°C. The initial discharge capacities for the samples calcined at 700, 750, 800, 850, and 900°C are 160.5, 167.8, 175.9, 184.3, and 189.2 $mAh \cdot g^{-1}$, respectively. A higher calcination temperature may enhance the crystallinity, which affects the insertion and extraction of lithium ions [39]. However, the sample calcined at 950°C only shows an initial discharge capacity of 178.3 $mAh \cdot g^{-1}$, possibly because of its large particles and particle aggregation. As shown in Fig. 4(b), the discharge capacities after 100 cycles are 144.6, 152.4, 154.0, 168.7, 177.8, and 155.9 $mAh \cdot g^{-1}$ for samples calcined at 700, 750, 800, 850, 900 and 950°C, respectively. Among these samples, the NCM622 sample calcined at 900°C delivers the best capacity performance with a high capacity retention of 94.0%, corresponding to retentions of 90.1%, 90.8%, 91.0%, 91.5%, and 87.4% of the materials calcined at 700, 750, 800, 850, and 950°C, respectively.

The electrochemical performance of the NCM622 samples at a 1C rate is shown in Fig. 5. From 0.2C to 1C rate, with increasing current density, the discharge capacity of the samples decreases. With increasing calcination temperature, the initial discharge capacity increases. The initial discharge capacity reaches 147.7, 151.5, 159.4, 167.1, 170.7, and 164.5 $mAh \cdot g^{-1}$ for the samples obtained at 700, 750, 800, 850, 900, and 950°C, respectively. The corresponding coulombic efficiency is 84.7%, 85.6%, 86.9%, 87.0%, 87.2%, and 83.0%, respectively. With increasing temperature, the difference between the charge and discharge plateau voltages increases, indicating increased polarization. The capacity retention after 100 cycles is 83.8%, 86.8%, 85.6%, 89.1%, 92.1%, and 82.5%, respectively. Notably, the material ob-

tained at 900°C exhibits the best cycle performance among the six samples.

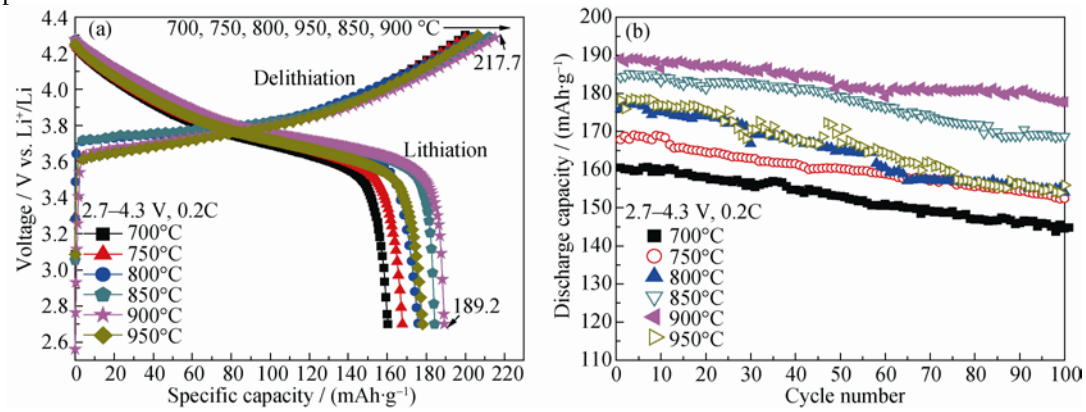


**Fig. 4. (a) Initial charge and discharge curves and (b) discharge capacities of NCM622 samples calcined at different temperatures and cycled between 2.7 and 4.3 V at a 0.2C rate.**

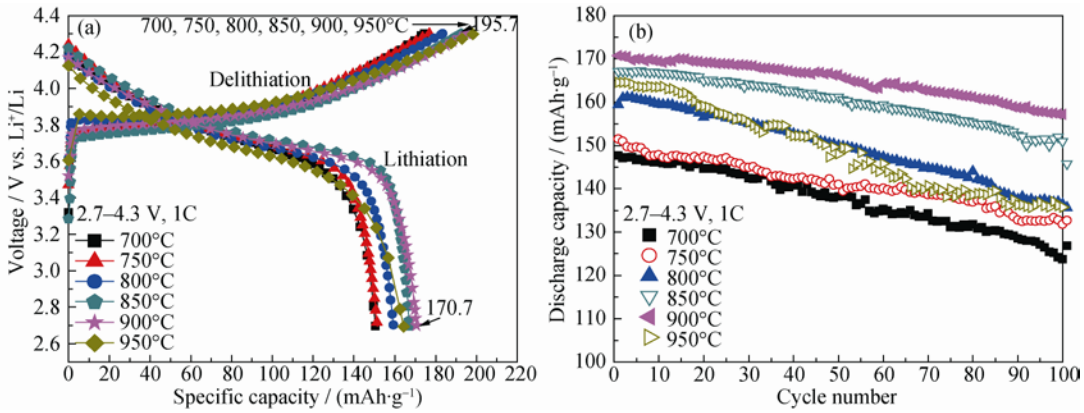


**Fig. 5. (a) Initial charge and discharge curves and (b) discharge capacities of the NCM622 samples calcined at different temperatures and cycled between 2.7 and 4.3 V at a 1C rate.**

Fig. 6 shows the rate capability of the NCM622 materials. All of the samples were tested at 0.1C, 0.2C, 0.5C, 1C, 2C, 5C, and then at 0.1C again for 10 cycles at each rate. With increasing current density, the discharge capacities of the samples decrease. As shown in Fig. 6, the material calcined at 900°C exhibits the best rate capability. It delivers a discharge capacity of 194.5, 185.1, 172.9, 159.6, 141.3, and 119.8 mAh·g$^{-1}$ at 0.1C, 0.2C, 0.5C, 1C, 2C, and 5C, respectively. Moreover, after being cycled from 0.1C to 5C, the recovered discharge capacity of 193.0 mAh·g$^{-1}$ at 0.1C is almost the same as the initial discharge capacity at 0.1C. These results indicate good structural stability of the sample calcined at 900°C. The excellent electrochemical performance of the NCM622 material calcined at 900°C is attributable to its well-ordered layered structure, homogeneous distribution, and spherical-like morphology.

The CV curves for the first three scans at a scan rate of 0.1 mV·s$^{-1}$ between 2.7 and 4.3 V are shown in Fig. 7. As displayed, the first scan curves differ from the subsequent two scans. The samples all show one redox couple between 3.6 and 4.0 V in the CV, which can be ascribed to the $Ni^{2+}/Ni^{4+}$ redox reaction. The peak potential difference of the sample calcined at 900°C (0.17 V) is less than those of the samples calcined at 700°C (0.39 V), 750°C (0.28 V), 800°C (0.27 V), 850°C (0.21 V), and 950°C (0.27 V), indicating that the sample calcined at 900°C exhibits the best electrochemical reversibility. In the two subsequent scans, the peak potential differences of the sample decrease compared with the first scan, which can be attributed to the

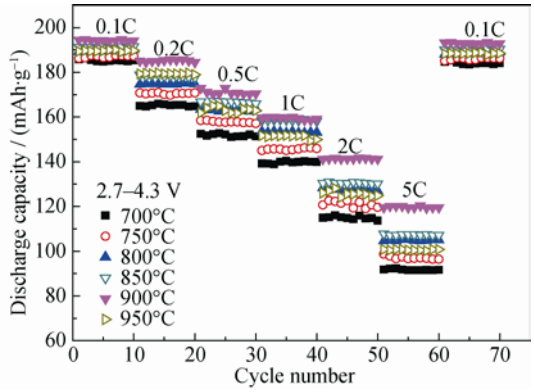


**Fig. 6. Rate performance of NCM622 samples calcined at different temperatures and cycled between 2.7 and 4.3 V.**

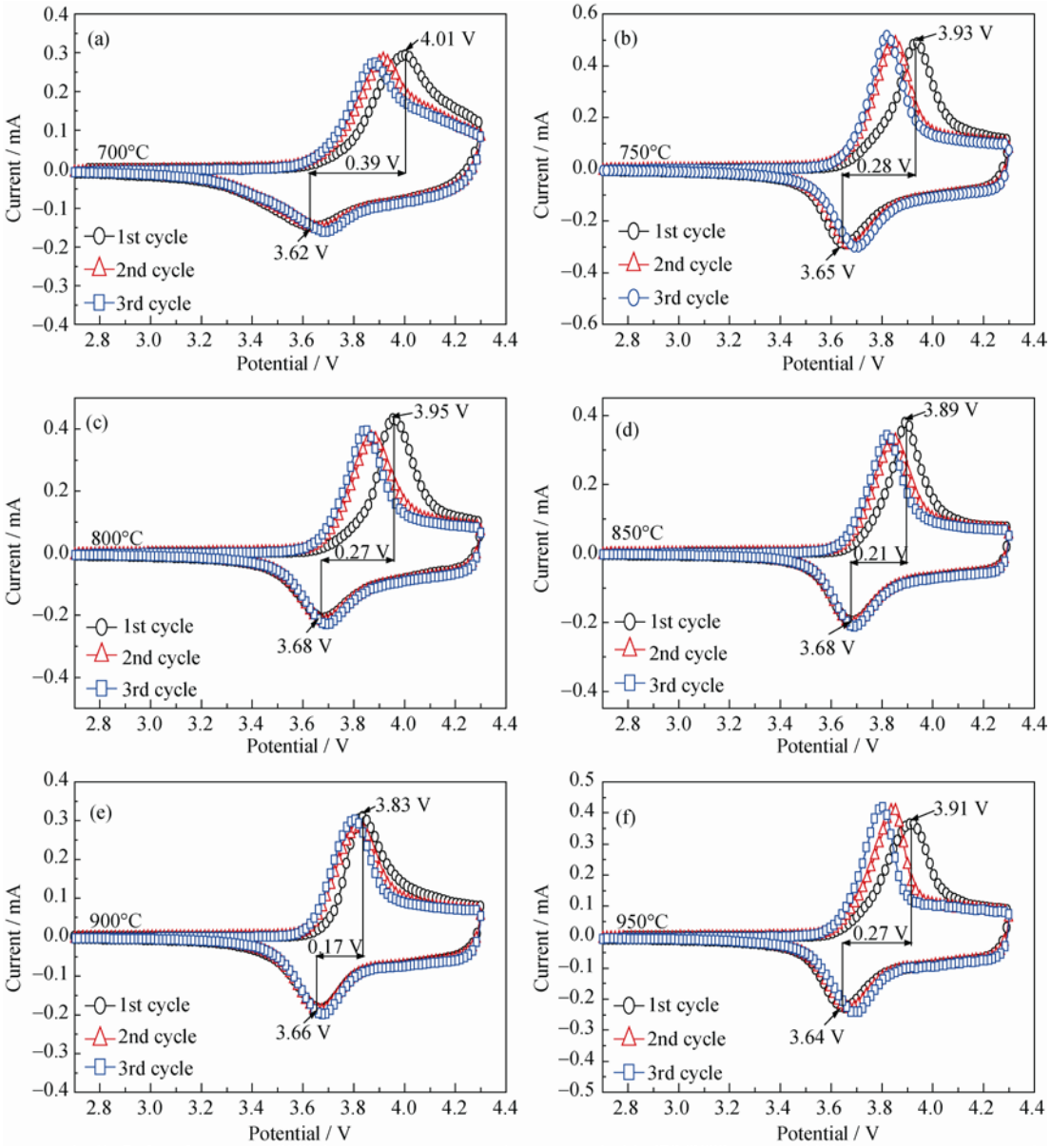


**Fig. 7. Cyclic voltammograms of the NCM622 materials obtained at different calcination temperatures with a scan rate of 0.1 $mV \cdot s^{-1}$ between 2.7 and 4.3 V.**

electrode activation, ameliorating the reaction reversibility. This result is in accordance with the excellent electrochem-

ical performance of this sample, as previously discussed.

3.2.2. Electrochemical performance of the NCM622 sample prepared at 900°C under different cut-off voltages

Furthermore, the electrochemical performance of the NCM622 sample prepared at 900°C under different charge cut-off voltages is shown in Figs. 8 and 9.

Fig. 8(a) shows the charge–discharge curves at the 1st and 100th cycles. The initial discharge capacity gradually increases with increasing charge cut-off voltage: 189.2, 197.7, and 208.3 mAh·g$^{-1}$ for 2.7–4.3, 2.7–4.4, and 2.7–4.5 V, respectively. The increased capacity percentage is 4.5% and 10.1% when the charge cut-off voltage is increased to 4.4 and 4.5 V, respectively, relative to the capacity at 4.3 V. At the 100th cycle, the discharge capacity is 177.8 mAh·g$^{-1}$ for 2.7–4.3 V, 173.8 mAh·g$^{-1}$ for 2.7–4.4 V, and 169.9 mAh·g$^{-1}$ for 2.7–4.5 V. The difference between charge and discharge plateau voltages also increases with the increasing charge cut-off voltage, suggesting that the increased polarization may promote electrolyte decomposition. Fig. 8(b) shows the cycling performance at 0.2C. After 100 cycles, the capacity retention is 94.0%, 87.9%, and 82.0% for 2.7–4.3 V, 2.7–4.4 V, and 2.7–4.5 V, respectively.

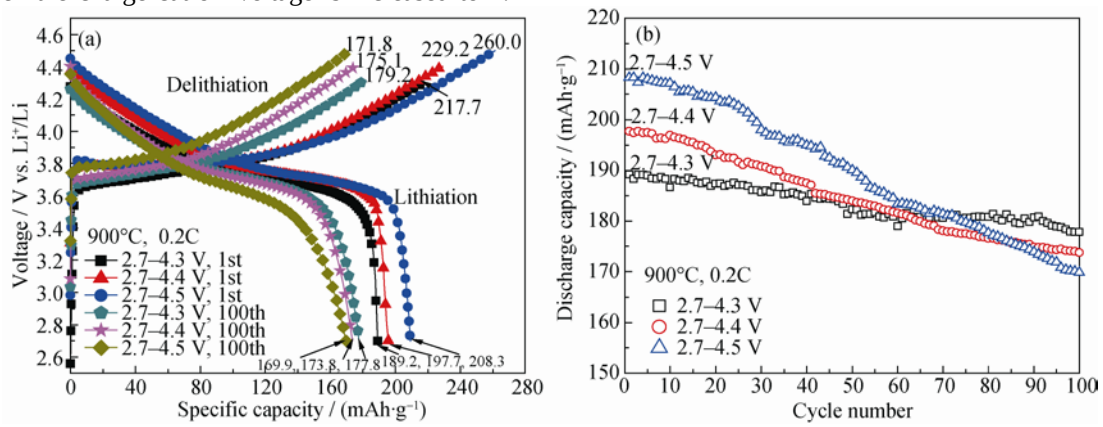


**Fig. 8. (a) Charge-discharge curves and (b) cycling performance with increasing charge cut-off voltage at a 0.2C rate for the NCM622 sample calcined at 900°C.**

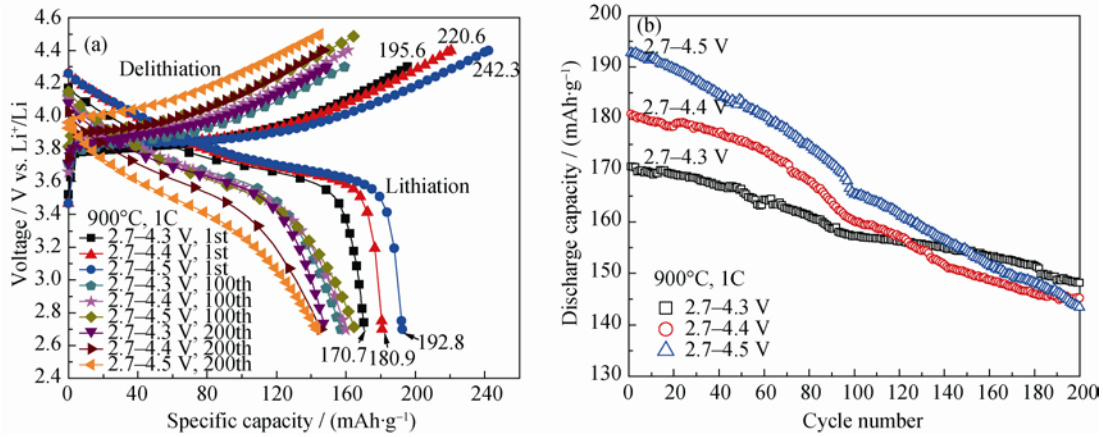


**Fig. 9. (a) Charge-discharge curves and (b) cycling performance with increasing charge cut-off voltage at a 1C rate for the NCM622 sample prepared at 900°C.**

Figs. 9(a) and 9(b) show the electrochemical performance at a 1C rate under different charge cut-off voltages. As displayed in Fig. 9(a), the initial discharge capacity increases with increasing charge cut-off voltage: 170.7, 180.9, and 192.8 mAh·g$^{-1}$, respectively. The corresponding coulombic efficiency is 87.3%, 82.0%, and 79.6%, respectively. The increased capacity percentage is 7.1% and 12.9% when the charge cut-off voltage is increased to 4.4 V and 4.5 V, respectively, relative to the capacity at a cut-off voltage of 4.3 V. Although a high charge cut-off voltage results in a higher capacity, it adversely affects cycling performance. With increasing number of cycles, the difference between charge and discharge plateau voltages increases. At the same number of cycles, such as the 100th cycle or the 200th cycle, the difference also increases with increasing charge cut-off voltage, which means diminished reaction reversibility. The

cycling stability of the material at 1C is shown in Fig. 9(b). After 100 cycles, the discharge capacity decreases from 170.7 to 157.2, 180.9 to 160.1, and 192.8 to 165.3 $mAh \cdot g^{-1}$ within the voltages of 2.7–4.3 V, 2.7–4.4 V, and 2.7–4.5 V, respectively. The discharge capacity at the 100th cycle between 2.7 and 4.4 (or 4.5 V) is higher than that between 2.7 and 4.3 V. The corresponding capacity retention is 92.1%, 88.5%, and 85.7%, respectively. The discharge capacity obviously decreases from the 100th cycle to the 200th cycle. The discharge capacity at the 200th cycle is 148.2, 145.2, and 143.4 $mAh \cdot g^{-1}$ for 2.7–4.3 V, 2.7–4.4 V, and 2.7–4.5 V, respectively. The capacity retention is 86.8%, 80.3%, and 74.4% after 200 cycles. The discharge capacity of the as-prepared NCM622 increases with increasing charge cut-off voltage; however, the cycling stability of the as-prepared NCM622 becomes worse. Side reactions and thermodynamic instability of cathode materials at high voltages (i.e., a high degree of lithium removal) diminished the cycling stability of the cathode material. Maintaining desirable crystal and electronic structures that enable efficient transport of electrons and ions for redox reactions at transition-metal sites is important for achieving a stable cycling performance for the NCM622 cathode material. Some studies [40–42] have shown that undesirable phase transformations that occur in cathodes can lead to failure in batteries cycled to high voltages. In particular, surface reconstruction (surface transition-metal reduction) from a layered structure to a mixed spinel/rock-salt structure is related to the high-voltage failure of the cathode material. The structure becomes unstable, and naturally unstable $Ni^{4+}$ ions are active at higher voltages; these ions can easily catalyze the oxidative decomposition of the electrolyte and ultimately lead to poor cycling performance of the battery [43]. The dissolution of transition-metal cations to the electrolyte also affects the cycling performance. The dissolution of cobalt at higher operating voltages (> 4.3 V) has been reported to be an important factor affecting cycling performance [30]. In our work, the as-prepared NCM622 cathode material exhibits good electrochemical performance, including long-term cycling stability, even under higher voltages; the long-term cycling stability of this material is superior to those of similar previously reported cathode materials [25,44]. The uniform spherical-like shape is beneficial to maintaining the structural stability of the material and to reducing Co dissolution [30]. In addition, the spherical-like morphology and uniform dispersion of the material could increase the tap-density, which is beneficial to the volume specific capacity of the material.

## 4. Conclusion

A spherical-like $Ni_{0.6}Co_{0.2}Mn_{0.2}(OH)_2$ precursor was controllably synthesized to tune the properties of NCM622 as a cathode material. The calcination temperature strongly affected the morphology, structure, and electrochemical performance of the as-synthesized NCM622 cathode material. The sample calcined at 900°C had the most extensively layered structure, with a particle size of approximately 10 μm. It delivered an initial discharge capacity of 189.2 $mAh \cdot g^{-1}$ at 0.2C with a capacity retention of 94.0% after 100 cycles between 2.7 and 4.3 V. It also exhibited good rate performance, with a capacity of 119.6 $mAh \cdot g^{-1}$ at 5C. Furthermore, it exhibited excellent cycling performance even under higher voltages. Within the voltage ranges from 2.7 to 4.3, 4.4, and 4.5 V, the initial discharge capacity at 1C reached 170.7, 180.9, and 192.8 $mAh \cdot g^{-1}$, respectively. The corresponding discharge capacity retention values were 86.8%, 80.3%, and 74.4% after 200 cycles, respectively.

## Acknowledgements

This project was financially supported by NSAF (No. U1530155), Ministry of Science and Technology (MOST) of China, US–China Collaboration on Cutting-edge Technology Development of Electric Vehicle, the Nation Key Basic Research Program of China (No. 2015CB251100), and Beijing Key Laboratory of Environmental Science and Engineering (No. 20131039031).

## References

[1] P. Gibot, M. Casas-Cabanas, L. Laffont, S. Levasseur, P. Carlach, S. Hamelet, J.M. Tarascon, and C. Masquelier, Room-temperature single-phase Li insertion/extraction in nanoscale $Li_xFePO_4$, *Nat. Mater.*, 7(2008), No. 9, p. 741.

[2] J.M. Tarascon and M. Armand, Issues and challenges facing rechargeable lithium batteries, *Nature*, 414(2001), No. 6861, p. 359.

[3] Z.G. Yang, J.L. Zhang, M.C.W. Kintner-Meyer, X.C. Lu, D. Choi, J.P. Lemmon, and J. Liu, Electrochemical energy storage for green grid, *Chem. Rev.*, 111(2011), No. 5, p. 3577.

[4] L.Y. Yu, W.H. Qiu, J.Y. Huang, and F. Lian, Synthesis and electrochemical characteristics of $xLi_2MnO_3 \cdot (1-x)Li(Ni_{1/3}Co_{1/3}Mn_{1/3})O_2$ compounds, *Int. J. Miner. Metall. Mater*, 16(2009), No. 4, p. 458.

[5] S.H. Yun, K.S. Park, and Y.J. Park, The electrochemical property of $ZrF_x$-coated $Li[Ni_{1/3}Co_{1/3}Mn_{1/3}]O_2$ cathode material, *J. Power Sources*, 195(2010), No. 18, p. 6108.

[6] J. Choi and A. Manthiram, Crystal chemistry and electrochemical characterization of layered $LiNi_{0.5-y}Co_{0.5-y}Mn_{2y}O_2$ and $LiCo_{0.5-y}Mn_{0.5-y}Ni_{2y}O_2$ ($0 \le 2y \le 1$) cathodes, *J. Power Sources*, 162(2006), No. 1, p. 667.

[7] M.H. Kim, H.S. Shin, D. Shin, and Y.K. Sun, Synthesis and electrochemical properties of $Li[Ni_{0.8}Co_{0.1}Mn_{0.1}]O_2$ and $Li[Ni_{0.8}Co_{0.2}]O_2$ via co-precipitation, *J. Power Sources*, 159(2006), No. 2, p. 1328.

[8] T. Ohzuku and Y. Makimura, Layered lithium insertion material of $LiCo_{1/3}Ni_{1/3}Mn_{1/3}O_2$ for lithium-ion batteries, *Chem. Lett.*, 30(2001), No. 7, p. 642.

[9] W.B. Luo, X.H. Li, and J.R. Dahn, Synthesis, characterization, and thermal stability of $Li[Ni_{1/3}Mn_{1/3}Co_{1/3-z}(MnMg)_{z/2}]O_2$, *Chem. Mater.*, 22(2010), No. 17, p. 5065.

[10] R. Santhanam and B. Rambabu, High rate cycling performance of $Li_{1.05}Ni_{1/3}Co_{1/3}Mn_{1/3}O_2$ materials prepared by sol–gel and co-precipitation methods for lithium-ion batteries, *J. Power Sources*, 195(2010), No. 13, p. 4313.

[11] Y. Chen, G.X. Wang, K. Konstantinov, H.K. Liu, and S.X. Dou, Synthesis and characterization of $LiCo_xMn_yNi_{1-x-y}O_2$ as a cathode material for secondary lithium batteries, *J. Power Sources*, 119-121(2003), p. 184.

[12] J.G. Li, L. Wang, Q. Zhang, and X.M. He, Synthesis and characterization of $LiNi_{0.6}Mn_{0.4-x}Co_xO_2$ as cathode materials for Li-ion batteries, *J. Power Sources*, 189(2009), No. 1, p. 28.

[13] P.Y. Liao, J.G. Duh, and S.R. Sheen, Microstructure and electrochemical performance of $LiNi_{0.6}Co_{0.4-x}Mn_xO_2$ cathode materials, *J. Power Sources*, 143(2005), No. 1-2, p. 212.

[14] Y. Zhang, H. Cao, J. Zhang, and B.J. Xia, Synthesis of $LiNi_{0.6}Co_{0.2}Mn_{0.2}O_2$ cathode material by a carbonate co-precipitation method and its electrochemical characterization, *Solid State Ionics*, 177(2006), No. 37, p. 3303.

[15] S.K. Zhong, L. Wei, Z.G. Zuo, X. Tang, and Y.H. Li, Synthesis and electrochemical performances of $LiNi_{0.6}Co_{0.2}Mn_{0.2}O_2$ cathode materials, *Trans. Nonferrous Met. Soc. China*, 19(2009), No. 6, p. 1499.

[16] C.L. Gan, X.H. Hu, H. Zhan, and Y.H. Zhou, Synthesis and characterization of $Li_{1.2}Ni_{0.6}Co_{0.2}Mn_{0.2}O_{2+\delta}$ as a cathode material for secondary lithium batteries, *Solid State Ionics*, 176(2005), No. 7-8, p. 687.

[17] J.J. Saavedra-Arias, N.K. Karan, D.K. Pradhan, A. Kumar, S. Nieto, R. Thomas, and R.S. Katiyar, Synthesis and electrochemical properties of $Li(Ni_{0.8}Co_{0.1}Mn_{0.1})O_2$ cathode material: *ex situ* structural analysis by Raman scattering and X-ray diffraction at various stages of charge–discharge process, *J. Power Sources*, 183(2008), No. 2, p. 761.

[18] P. Yue, Z.X. Wang, H.J. Guo, F.X. Wu, Z.J. He, and X.H. Li, Effect of synthesis routes on the electrochemical performance of $Li[Ni_{0.6}Co_{0.2}Mn_{0.2}]O_2$ for lithium ion batteries, *J. Solid State Electr.*, 16(2012), No. 12, p. 3849.

[19] P. Yue, Z.X. Wang, W.J. Peng, L.J. Li, W. Chen, H.J. Guo, and X.H. Li, Spray-drying synthesized $LiNi_{0.6}Co_{0.2}Mn_{0.2}O_2$ and its electrochemical performance as cathode materials for lithium ion batteries, *Powder Technol.*, 214(2011), No. 3, p. 279.

[20] P. Yue, Z.X. Wang, W.J. Peng, L.J. Li, H.J. Guo, X.H. Li, Q.Y. Hu, and Y.H. Zhang, Preparation and electrochemical properties of submicron $LiNi_{0.6}Co_{0.2}Mn_{0.2}O_2$ as cathode material for lithium ion batteries, *Scripta Mater.*, 65(2011), No. 12, p. 1077.

[21] G.T.K. Fey, J.G. Chen, Z.F. Wang, H.Z. Yang, and T.P. Kumar, Saturated linear dicarboxylic acids as chelating agents for the sol–gel synthesis of $LiNi_{0.8}Co_{0.2}O_2$, *Mater. Chem. Phys.*, 87(2004), No. 2-3, p. 246.

[22] G.T.K. Fey, V. Subramanian, and C.Z. Lu, Tartaric acid-assisted sol–gel synthesis of $LiNi_{0.8}Co_{0.2}O_2$ and its electrochemical properties as a cathode material for lithium batteries, *Solid State Ionics*, 152(2002), p. 83.

[23] H.Q. Lu, H.T. Zhou, A.M. Svensson, A. Fossdal, E. Sheridan, S.G. Lu, and F. Vullum-Bruer, High capacity $Li[Ni_{0.8}Co_{0.1}Mn_{0.1}]O_2$ synthesized by sol–gel and co-precipitation methods as cathode materials for lithium-ion batteries, *Solid State Ionics*, 249(2013), p. 105.

[24] H. Cao, Y. Zhang, J. Zhang, and B.J. Xia, Synthesis and electrochemical characteristics of layered $LiNi_{0.6}Co_{0.2}Mn_{0.2}O_2$ cathode material for lithium ion batteries, *Solid State Ionics*, 176(2005), No. 13-14, p. 1207.

[25] L.W. Liang, K. Du, Z.D. Peng, Y.B. Cao, J.G. Duan, J.B. Jiang, and G.R. Hu, Co-precipitation synthesis of $Ni_{0.6}Co_{0.2}Mn_{0.2}(OH)_2$ precursor and characterization of $LiNi_{0.6}Co_{0.2}Mn_{0.2}O_2$ cathode material for secondary lithium batteries, *Electrochim. Acta*, 130(2014), p. 82.

[26] D.P. Abraham, R.D. Twesten, M. Balasubramanian, I. Petrov, J. McBreen, and K. Amine, Surface changes on $LiNi_{0.8}Co_{0.2}O_2$ particles during testing of high-power lithium-ion cells, *Electrochem. Commun.*, 4(2002), No. 8, p. 620.

[27] Y. Cho, P. Oh, and J. Cho, A new type of protective surface layer for high-capacity Ni-based cathode materials: nanoscaled surface pillaring layer, *Nano Lett.*, 13(2013), No. 3, p. 1145.

[28] M.M. Thackeray, C.S. Johnson, J.T. Vaughey, N. Li, and S.A. Hackney, Advances in manganese-oxide 'composite' electrodes for lithium-ion batteries, *J. Mater. Chem.*, 15(2005), No. 23, p. 2257.

[29] D. Aurbach, Review of selected electrode–solution interactions which determine the performance of Li and Li ion batteries, *J. Power Sources*, 89(2000), No. 2, p. 206.

[30] M.H. Lee, Y.J. Kang, S.T. Myung, and Y.K. Sun, Synthetic optimization of $Li[Ni_{1/3}Co_{1/3}Mn_{1/3}]O_2$ via co-precipitation, *Electrochim. Acta*, 50(2004), No. 4, p. 939.

[31] J.R. Ying, C.R. Wan, C.Y. Jiang, and Y.X. Li, Preparation and characterization of high-density spherical $LiNi_{0.8}Co_{0.2}O_2$ cathode material for lithium secondary batteries, *J. Power Sources*, 99(2001), No. 1-2, p. 78.

[32] J.Z. Kong, H.F. Zhai, C. Ren, G.A. Tai, X.Y. Yang, F. Zhou, H. Li, J.X. Li, and Z. Tang, High-capacity

$Li(Ni_{0.5}Co_{0.2}Mn_{0.3})O_2$ lithium-ion battery cathode synthesized using a green chelating agent, *J. Solid State Electrochem.*, 18(2013), No. 1, p. 181.

[33] D. Mohanty and H. Gabrisch, Microstructural investigation of $Li_xNi_{1/3}Mn_{1/3}Co_{1/3}O_2$ ($x \leq 1$) and its aged products via magnetic and diffraction study, *J. Power Sources*, 220(2012), p. 405.

[34] W.H. Ryu, S.J. Lim, W.K. Kim, and H.S. Kwon, 3-D dumbbell-like $LiNi_{1/3}Mn_{1/3}Co_{1/3}O_2$ cathode materials assembled with nano-building blocks for lithium-ion batteries, *J. Power Sources*, 257(2014), p. 186.

[35] D. Li, F. Lian, X.M. Hou, and K.C. Chou, Reaction mechanisms for $0.5Li_2MnO_3 \cdot 0.5LiMn_{0.5}Ni_{0.5}O_2$ precursor prepared by low-heating solid state reaction, *Int. J. Miner. Metall. Mater.*, 19(2012), No. 9, p. 856.

[36] K.M. Shaju, G.V.S. Rao, and B.V.R. Chowdari, Performance of layered $Li(Ni_{1/3}Co_{1/3}Mn_{1/3})O_2$ as cathode for Li-ion batteries, *Electrochim. Acta*, 48(2002), No. 2, p. 145.

[37] L.W. Liang, K. Du, Z.D. Peng, Y.B. Cao, and G.R. Hu, Synthesis and electrochemical performance of $LiNi_{0.6}Co_{0.2}Mn_{0.2}O_2$ as a concentration-gradient cathode material for lithium batteries, *Chin. Chem. Lett.*, 25(2014), No. 6, p. 883.

[38] J.N. Reimers, E. Rossen, C.D. Jones, and J.R. Dahn, Structure and electrochemistry of $Li_xFe_yNi_{1-y}O_2$, *Solid State Ionics*, 61(1993), No. 4, p. 335.

[39] J. Eom, M.G. Kim, and J. Cho, Storage characteristics of $LiNi_{0.8}Co_{0.1+x}Mn_{0.1-x}O_2$ ($x$ = 0, 0.03, and 0.06) cathode materials for lithium batteries, *J. Electrochem. Soc.*, 155(2008), No. 3, p. 239.

[40] S.K. Jung, H. Gwon, J. Hong, K.Y. Park, D.H. Seo, H. Kim, J. Hyun, W. Yang, and K. Kang, Understanding the degradation mechanisms of $LiNi_{0.5}Co_{0.2}Mn_{0.3}O_2$ cathode material in lithium ion batteries, *Adv. Energy Mater.*, 4(2014), No. 1.

[41] F. Lin, I.M. Markus, D. Nordlund, T.C. Weng, M.D. Asta, H.L. Xin and M.M. Doeff, Surface reconstruction and chemical evolution of stoichiometric layered cathode materials for lithium-ion batteries, *Nat. Commun.*, 5(2014).

[42] F. Lin, D. Nordlund, Y.Y. Li, M.K. Quan, L. Cheng, T.C. Weng, Y.J. Liu, H.L. Xin, and M.M. Doeff, Metal segregation in hierarchically structured cathode materials for high-energy lithium batteries, *Nat. Energy*, 1(2016), art. No. 15004.

[43] Y.S. Lee, D. Ahn, Y.H. Cho, T.E. Hong, and J. Cho, Improved rate capability and thermal stability of $LiNi_{0.5}Co_{0.2}Mn_{0.3}O_2$ cathode materials via nanoscale $SiP_2O_7$ coating, *J. Electrochem. Soc.*, 158(2011), No. 12, p. 1354.

[44] P. Yue, Z.X. Wang, X.H. Li, X. Xiong, J.X. Wang, X.W. Wu, and H.J. Guo, The enhanced electrochemical performance of $LiNi_{0.6}Co0.2Mn_{0.2}O_2$ cathode materials by low temperature fluorine substitution, *Electrochim. Acta*, 95(2013), p. 112.